Original

Kramm, U.I.; Herrmann-Geppert, I.; Fiechter, S.; Zehl, G.; Zizak, I.;
Dorbrandt, I.; Schmeisser, D.; Bogdanoff, P.:

Effect of iron-carbide formation on the number of active sites in Fe–N–C catalysts for the oxygen reduction reaction in acidic media

In: Journal of Materials Chemistry A (2013) Royal Society of Chemistry

DOI: 10.1039/c3ta13821f

Journal of Materials Chemistry A

PAPER

View Article Online
View Journal | View Issue

Cite this: J. Mater. Chem. A, 2014, 2, 2663

Effect of iron-carbide formation on the number of active sites in Fe–N–C catalysts for the oxygen reduction reaction in acidic media†

Ulrike I. Kramm,*[ab] Iris Herrmann-Geppert,[ac] Sebastian Fiechter,[a] Gerald Zehl,[a] Ivo Zizak,[d] Iris Dorbandt,[a] Dieter Schmeißer[b] and Peter Bogdanoff[a]

Received 23rd September 2013
Accepted 3rd December 2013

DOI: 10.1039/c3ta13821f

www.rsc.org/MaterialsA

In this work Fe–N–C catalysts were prepared by the oxalate-supported pyrolysis of FeTMPPCl or H_2TMPP either in the presence or absence of sulfur. The well-known enhancing effect of sulfur-addition on the oxygen reduction activity was confirmed for these porphyrin precursors. The pyrolysis process was monitored *in situ* by high-temperature X-ray diffraction under synchrotron radiation (HT-XRD) and thermogravimetry coupled with mass-spectroscopy (TG-MS). It was found that the beneficial effect of sulfur could be attributed to the prevention of iron-carbide formation during the heat-treatment process. In the case of pyrolysis of the sulfur-free precursors an excessive iron-carbide formation leads to disintegration of FeN_4-centers, hence limiting the number of ORR active sites on the final catalyst. Physical characterization of the catalysts by bulk elemental analysis, X-ray diffraction (XRD), Raman and ^{57}Fe Mößbauer spectroscopy confirmed the outcome from HT-XRD and TG-MS. It could be shown that the avoidance of carbide formation during pyrolysis represents a promising way to enhance the density of ORR active sites on those catalysts. This can be done either by sulfur-addition or the performance of an intermediate acid leaching. As iron carbide is often found as a by-product in the preparation of Fe–N–C catalysts this work gives some general strategies for enhancing the density of active sites enabling higher current densities.

Introduction

For automotive application the utilization of Polymer-Electrolyte-Membrane Fuel Cells (PEM-FC) as power sources is one of the most promising techniques especially in sparsely populated areas of *e.g.* North America. State-of-the-art catalysts are carbon-supported platinum (Pt/C) or its alloys. While platinum is an excellent catalyst for the hydrogen oxidation reaction (HOR) it reveals only a sluggish performance for the oxygen reduction reaction (ORR). Therefore, most of the platinum in today's fuel cells is used for the cathode, in order to get the reaction run.

However, for economic reasons catalyst costs have to be reduced as they contribute 33% to the overall costs of a FC stack.[1] The most effective would be the replacement of platinum by cheap non-noble metal catalysts (NNMCs). The most promising alternatives are the so-called Fe–N–C catalysts. Recent results demonstrate that these catalysts can indeed compete against platinum in terms of ORR activity, while their long-term performance has to be improved.[2–4]

The oxalate-supported pyrolysis has proven to be quite effective in the preparation of Me–N–C catalysts.[5–10] Especially in terms of active site density this technique is beneficial as no additional carbon support is required.[5] In previous work we demonstrated that (i) different oxalates[6] and (ii) different porphyrins can be utilized in this preparation.[10,11] The achievable activity depends on the optimized combination of both. The two most important steps in improving the ORR activity of these catalysts were the findings that much higher current densities are reached when sulfur is added to the precursor mixture of porphyrin plus iron oxalate[7,12] and that a second heat-treatment can drastically enhance the ORR activity.[8,9,11]

[a]Helmholtz-Centre Berlin for Materials and Energy, Institute of Solar Fuels, Hahn-Meitner-Platz 1, 14109 Berlin, Germany

[b]Brandenburgische Technische Universität Cottbus-Senftenberg, Chair of Applied Physics and Sensors, Konrad-Wachsmann-Allee 17, 03046 Cottbus, Germany. E-mail: kramm@tu-cottbus.de; Tel: +49-355-69-2972

[c]Helmut-Schmidt-University, Functional Materials, Holstenhofweg 85, 22043 Hamburg, Germany, Helmholtz Centre Geesthacht, Institute for Materials Research, Max-Planck-Str. 1, 21502 Geesthacht, Germany

[d]Helmholtz-Centre Berlin for Materials and Energy, BESSY II, Albert-Einstein-Str. 15, 12489 Berlin, Germany

† Electronic supplementary information (ESI) available: Detailed discussion of the pyrolysis process of the FeTMPPCl + iron-oxalate-dihydrate precursors with and without sulfur by TG-MS and selected diffractograms of HT-XRD measurements; physical characterization of the H_2/Fe + S and H_2/Fe – S catalysts (by XRD, Raman spectroscopy and Mößbauer spectroscopy); table summarizing the Mößbauer parameters and assignments to iron species of all standard catalysts; TEM images of the Fe/Fe – S catalyst; RDE measurements with 200, 400, and 900 rpm of all standard catalysts. Comparison of the effect of second heat-treatment in either N_2 or NH_3, respectively, on the ORR activity of the reference catalyst and Fe/Fe + S. See DOI: 10.1039/c3ta13821f

The performance of this second heat-treatment in different gas atmospheres enabled the preparation of catalysts with different ORR activities and various concentrations of iron species as determined by ^{57}Fe Mößbauer spectroscopy.[8] This approach enabled a direct correlation between one specific FeN_4-center and the ORR activity. In a recent publication we have shown that the turn-over frequency related to this active site depends on the electron density on the iron center.[13] It can be tuned for instance by a change of the pyrolysis temperature.

Regarding the amount of sulfur to be added, the ratio of sulfur to iron has to be optimized as undersized ratios might not enable optimal improvement while an oversized sulfur quantity will cause the formation of FeS_x ($x > 1$) type phases with poor solubility in acidic medium.[14] For example, although acid-leached at boiling temperature, the so called PANI–Fe–C catalysts exhibit large concentrations of Fe_3S_4 which can be explained by the reaction of ammonium peroxidisulfate (APS) residuals (from the polymerization step) with the iron source.[15] A beneficial effect of sulfur on the ORR activity of Me–N–C catalysts was also described by Contamin *et al.* and Hatchard *et al.*[16,17]

Catalysts prepared by the oxalate-supported pyrolysis under sulfur-addition exhibited the best performance in RDE experiments in a cross-laboratory comparison of different institutes worldwide.[18] In this publication the activity was enhanced by a multi-step preparation. After the first heat-treatment in inert gas followed by acid-leaching, a second heat-treatment in forming gas with subsequent acid-leaching and a third heat-treatment in CO_2 were applied.[18]

The catalysts discussed in this work were also prepared by the oxalate-supported pyrolysis, but characterized just after the first heat-treatment plus acid-leaching. This is because the focus of this work was not to beat all previous results with respect to ORR activity, but to elucidate the reason for the different performance of catalysts prepared by this technique with and without sulfur-addition to the precursor mixture.

Experimental

I. Preparation of Fe–N–C catalysts

Precursor preparation (±S). In order to prepare a sulfur-free precursor, 1.3 mmol FeTMPPCl (TriPorTech, 95% purity) was mixed with 28.6 mmol iron-oxalate dihydrate (Riedel de Häen) in a mortar until a homogeneous precursor mixture was obtained. To prepare a sulfur-containing precursor 1.2 mmol sulfur (S_8) were ground previously before mixing with the oxalate and FeTMPPCl. This molar ratio of sulfur to metal was previously found to give the best results in terms of activity improvement and removal of inorganic metal species.[14]

These precursors were used for the preparation of the standard catalysts and the catalysts with intermediate acid leaching. In addition, to elucidate the processes involved in catalyst formation, small quantities of these mixtures were used for the *in situ* investigation of the heat treatment process (HT-XRD and TG-MS measurements).

Preparation of the standard catalysts (±S). Each precursor was filled in a quartz boat, placed in a quartz glass tube and heated from room temperature to 800 °C. The heating rate was 7.5 °C min^{-1}. At 450 °C the samples were held for 10 min before they were heated to 800 °C and held at this temperature for 45 min. The complete heat treatment process was performed in a nitrogen atmosphere. After quenching to room temperature (RT), the samples were transferred into 1 M hydrochloric acid and stirred for at least 1 h in an ultrasonic bath. The catalysts were filtered and washed with distilled water until the filtrate exhibited a pH value of 5. The obtained black catalyst powders were dried at 80 °C. The final catalysts prepared by the pyrolysis of FeTMPPCl and iron-oxalate dihydrate without or with sulfur-addition will be addressed "Fe/Fe − S" and "Fe/Fe + S", respectively.

In a similar way catalysts were prepared by the oxalate-supported pyrolysis of H_2TMPP, utilizing the same molar ratios as given above. These catalysts are labelled "H_2/Fe − S" and "H_2/Fe + S".

Preparation of the reference catalysts (Fe/KB600). The electrochemical behavior of the prepared catalysts was compared to that of an impregnation catalyst. The detailed preparation is described by Koslowski *et al.* (ref. 8). In short, FeTMPPCl was impregnated on Ketjen Black 600 and subjected to a heating process with 800 °C as the end temperature (5 °C min^{-1}) followed by a subsequent acid leaching similar to that of the catalysts prepared by the standard preparation technique. This catalyst is labelled as "Fe/KB600".

Preparation of catalysts with intermediate acid leaching (±S). In order to verify the findings related to the role of iron-carbide formation during the preparation process, the standard preparation was modified. The precursor mixtures remained the same as for the standard catalysts, but treatment in an acidic solution as an intermediate step was added.

Each precursor was filled in a quartz boat, placed in a quartz glass tube and heated from room temperature to 500 °C (30 min) in a first step. After cooling down the samples were acid-leached in 1 M HCl, similar to the procedure described above. After drying the intermediates, these were filled again into quartz boats and heated from room temperature to 800 °C, at which the temperature was maintained for 30 min. After cooling down to room temperature (RT), again the samples were acid-leached. Both heat-treatment steps were performed in a nitrogen atmosphere with a heating rate of 7.5 °C min^{-1}. As the main difference in comparison to the standard preparation is the intermediate acid leaching, these catalysts are labelled as "Fe/Fe − S + IAL" and "Fe/Fe + S + IAL".

II. *In situ* characterization of the pyrolysis process

***In situ* high-temperature X-ray diffraction measurements (HT-XRD).** In order to analyse the solid products that are formed during the heating process, *in situ* X-ray diffraction measurements were performed at the BESSY II beam line KMC-2 using a stainless-steel reaction chamber with Kapton® windows at the beam entry and exit slits. The precursor samples were placed on an electric graphite heater encapsulated in pyrolytic boron nitride (pBN) from Tectra GmbH. This newly developed reaction chamber is shown in Fig. 1 and allows measurements under constant Ar gas flow at reduced pressures in a temperature range from RT to 800 °C applying a heating rate of 7.5 K min^{-1}.[19] A two dimensional detector array (HiStar – Bruker AXS) was used to record the spectra.

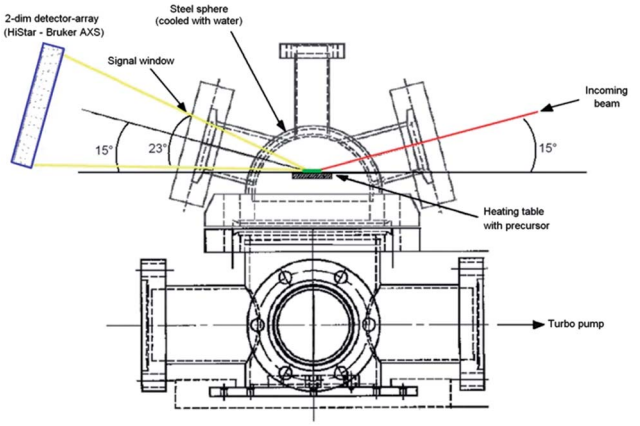

Fig. 1 Reaction chamber for high-temperature X-ray diffraction measurements as performed at the KMC-2 beamline at BESSY II.

The detector, sample and synchrotron-radiation beam were aligned to meet the Bragg–Brentano geometry. To simulate the heating process, measurements were carried out under a constant Ar flow of 200 ml min^{-1} at a reduced pressure of $p = 400$ mbar. X-ray source synchrotron radiation with an energy of 8.731 keV was applied. Calibration of the system was performed using an alumina standard. Because of the reduced pressure, the precursor samples were pelletized (Ø: 10 mm) before placing onto the pBN heating table.

For easier comparison to the X-ray diffractograms of the standard catalysts, the 2θ-values of the XRD peak positions measured with different X-ray sources were referred and compared with those taken at the wavelength of a Cu Kα X-ray tube as shown in Fig. 2c and d and S2.†

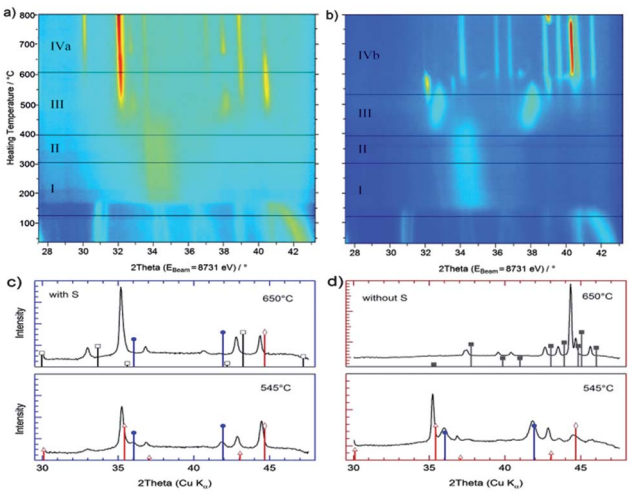

Fig. 2 HT-XRD measurements of the FeTMPPCl + iron oxalate dihydrate precursor mixture with sulfur (a and c) and without sulfur (b and d). Dark blue color denotes low intensity regions and the continuous change to red color indicates an increase of the signal intensity. In (c) and (d) the X-ray diffractograms as obtained at 545 °C and 650 °C are shown. Diffraction patterns can be assigned to troilite FeS (□), wüstite FeO (●), alpha iron (◊), magnetite (Δ), and cohenite Fe_3C (■).

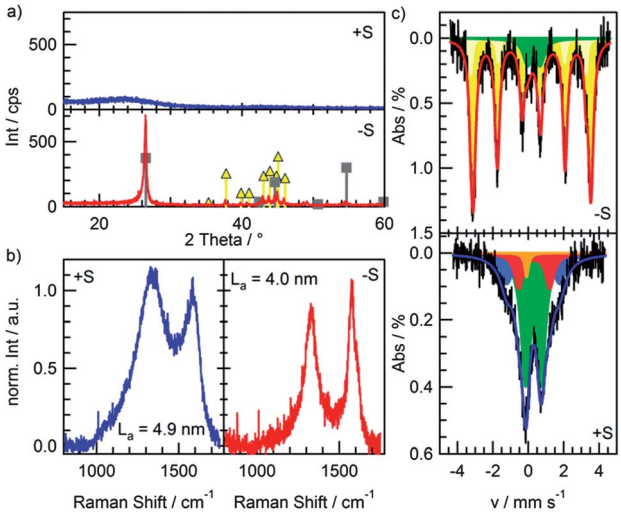

Fig. 3 X-ray diffraction (a), Raman measurements (b) and Mößbauer spectra of the final Fe/Fe − S and Fe/Fe + S catalysts after pyrolysis up to 800 °C followed by a subsequent acid leaching are given. Diffraction patterns can be assigned to cohenite Fe_3C (Δ) and graphite (■). The Mößbauer parameters and assignment to iron species are summarized in Table S2 in the ESI.†

Thermogravimetry coupled with mass-spectroscopy (TG-MS). Thermogravimetric measurements were carried out at the Institut für Kristallzüchtung (IKZ) using a NETZSCH Simultaneous Thermal Analyzer STA 409C coupled with a quadrupole mass spectrometer *via* a skimmer. The measurements were performed in an Al_2O_3 sample crucible under continuous flow of helium with a heating rate of 7.5 K min^{-1}.

III. Characterization of the final catalysts

Electrochemical characterization. Catalyst inks have been prepared by suspending 2 mg of catalyst in 400 µl of a 1 : 1 water–ethanol mixture containing 0.2% Nafion. 5 µl of this suspension were dropped onto a 0.1963 cm^2 glassy carbon disk (RDE) obtaining a catalyst load of 0.13 mg cm^{-2}. The experiments were carried out at room temperature in a three-electrode-system with a platinum wire as the counter electrode and Hg/Hg_2SO_4/0.5 M H_2SO_4 as the reference electrode (0.68 V *vs.* SHE).

Prior to the determination of the oxygen reduction current the working electrode with our catalyst was cycled in a potential range from 1.0 V to 0.0 V with a scan rate of 50 mV s^{-1} in nitrogen-saturated 0.5 M H_2SO_4. Typically 15–20 scans were required until a steady state was reached. In the CV diagrams of Fig. 4a and 5a always the last scans out of this line are displayed. Previous to the RDE experiments, the electrolyte was purged with oxygen and the open circuit potential (OCP) was measured. RDE experiments were performed with a sweep rate of 5 mV s^{-1} in an oxygen-saturated electrolyte at 200, 400, 576, 729 and 900 rpm (in this sequence). During the measurement, oxygen was only passed over the surface of the electrolyte. Tafel plots have been calculated by the Levich approach. All potentials are given in reference to the standard hydrogen electrode (SHE).

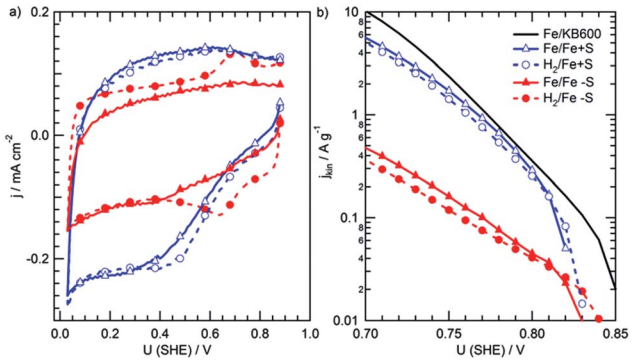

Fig. 4 Cyclic voltammograms (a) and Tafel plots (b) of the catalysts prepared without and with sulfur in the precursor mixtures.

Elemental analysis. In order to determine the elemental composition of the catalysts neutron activation analysis (NAA) and combustion analysis were made to determine the iron contents and the mass-related contents of carbon, nitrogen, sulfur and hydrogen, respectively.

X-ray diffraction. For the identification of crystalline phases, XRD measurements of all standard catalysts were carried out employing a Bruker diffractometer D8 Advance in Bragg–Brentano θ–2θ coupling using Cu Kα radiation (λ = 1.54 Å) and a silicon disk as the sample holder. Samples were rotated during the measurements. Spectra were recorded in a range of $15° < 2\Theta < 60°$. The measured diffractograms were analyzed using the database of the Joint Committee on Powder Diffraction Standards (JCPDS).

Raman spectroscopy. To characterize the carbon structure, Raman measurements were performed in a range from 1750 to 800 cm^{-1} using a He/Ne laser for the excitation. The catalyst powders were suspended in water and small amounts of these suspensions were dropped onto glass substrates and left to dry. By this treatment flat films of the catalyst powders were obtained on which the laser beam was focused with the help of an optical microscope (Olympus BX). In order to separate Raman and Rayleigh scattering a notch filter and a monochromator were utilized. Raman bands were detected with a CCD camera. For each sample measurements were performed in two different sample areas and the sum spectra were analyzed. Following the semi-empirical equation by Tuinstra and König,[20] the graphene layer extensions were calculated:

$$L_a = I_{D\text{-peak}}/I_{G\text{-peak}} \times 4.4 \text{ nm}$$

^{57}Fe Mößbauer spectroscopy. Mößbauer measurements were made to characterize the iron compounds within each standard catalyst. The spectra were recorded at room temperature with a CMCA-550 (Wissel) equipped with a constant electronic drive system with a triangular reference waveform (Halder Electronics). A ^{57}Co/Rh-source was used, and the velocity scale and isomer shift δ_{iso} were calibrated with natural iron (α-Fe-foil, 25 μm thick, 99.99% purity). An assignment of the iron species was made by a comparison of the Mößbauer parameters to literature data.

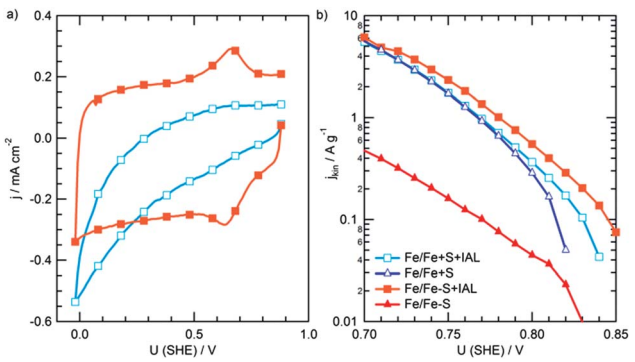

Fig. 5 Cyclic voltammograms of the catalysts prepared by the oxalate-supported pyrolysis of FeTMPPCl with intermediate acid leaching (+IAL) (a) and comparison of the Tafel plots of the catalysts obtained by the standard method and the modified preparation route.

Results

I. Analysis of the pyrolysis process

In order to investigate the pyrolysis process thermogravimetry coupled with mass-spectroscopy (TG-MS) and high-temperature X-ray diffractometry (HT-XRD) were performed for the FeTMPPCl + iron oxalate dihydrate precursor with and without sulfur-addition. In our previous work, TG-MS measurements of different CoTMPP-oxalate precursors have been already described.[6,7] Therefore, only the major differences induced by the addition of sulfur are summarized here, while in the ESI† the TG-MS results are discussed in detail, see Fig. S1.†

First of all, for both precursors the pyrolysis process can be divided into four sections separated from each other by the release of characteristic gas species. Up to 500 °C the thermogravimetric curves appeared to be quite similar. However,

(i) above 500 °C the third (and final) decomposition step was shifted from 550 °C (as obtained for the sulfur-free precursor) to 750 °C for the sulfur-added precursor (see the TG-part of Fig. S1†).

(ii) Due to sulfur-addition, a strong release of gaseous sulfur species detected as positively charged fragments in the mass spectrometer were found in the temperature range from 300 to 700 °C (m/z = 64 in Fig. S1†).

(iii) The mass-fragments related to the decomposition of MeN$_4$-centers (HCN, N$_2$) showed a single peak for the sulfur-containing precursor (450–520 °C), whereas an additional decomposition peak was observed between 550 and 650 °C for the sulfur-free precursor (m/z = 27, 28 in Fig. S1†).

The *in situ* HT-XRD measurements shown in Fig. 2 approve that these differences are basically due to the formation of different intermediates during the heating process. Fig. 2a and b show the overview of the measurements obtained at temperatures between RT and 800 °C for both precursors. The four different temperature ranges are indicated by roman letters. Note that, caused by a thermal-induced expansion of the crystalline phases at higher temperatures the reflections are shifted to smaller 2θ-angles. In the ESI (Fig. S2†) the extracted

diffractograms are given for several temperatures that are representative for the heating processes (usually before and after a main decomposition step).

Due to the high amount of iron oxalate dihydrate in the precursor mixture compared to the quantity of porphyrin, the diffractogram of the starting material (RT) is dominated by the diffraction reflections of the oxalate. In agreement with the TG-MS measurements the HT-XRD measurements are similar up to a heat-treatment temperature of 500 °C. Going from the temperature regime I to II (150 °C–200 °C) the iron-oxalate dihydrate releases its crystal water and the characteristic diffraction patterns of iron oxalate are found at $T > 200$ °C. In agreement with the thermogravimetric measurements iron oxalate starts to decompose at *ca.* 400 °C and forms iron-oxide phases (wüstite and magnetite) which can be identified by the diffraction patterns at 435 °C and even more pronounced at 545 °C (see Fig. 2c and d). From previous investigations it is known that in the range from 400 to 450 °C also the carbonization of the porphyrin precursor is initiated.[5–7,21] In the temperature range 545 °C to 650 °C the reduction of the oxides begins initiated by the *in situ* formed carbon. This temperature range seems the most important one related to the changes observed for both final catalysts. Therefore, the XRD diffractograms of both precursors are given after heating to 545 and 650 °C in Fig. 2c and d, respectively.

For the sulfur-free precursor (Fig. 2d), at 650 °C the formation of iron carbide (cohenite) as a reaction product became dominant caused by the reduction of iron oxides formed in the temperature region before.

$$3FeO + C \rightarrow Fe_3C + 3/2O_2$$

It is important to note that this is the same temperature range where the additional release of HCN (545 °C–650 °C) was found (compare main difference (iii)) in TG-MS as discussed above. Between 680 °C and 800 °C the intensity ratio of the cohenite reflections varies indicating a change in crystal structure.[22]

In contrast to the precursor mixture without sulfur, the carbide formation in the sulfur-containing precursor is inhibited, as can be seen in Fig. 2c. The main phases found in the diffractograms are troilite (FeS) and wüstite (FeO). Apparently, sulfur reacts with the iron compounds to form iron sulfide and suppresses the formation of iron carbide. We will come back to this observation in the discussion part.

In a standard preparation route, the so gained pyrolysis products were conditioned in a subsequent acid leaching (1 h under ultrasonic treatment in 1 M HCl at 25 °C) in order to remove inactive by-products.

II. Influence of the sulfur-addition on the structural composition of the final catalysts

The X-ray diffractograms, Raman and Mößbauer spectroscopic measurements of the final conditioned catalysts (after pyrolysis (800 °C), acid leaching and washing, compare with the Experimental section) are given in Fig. 3 for the FeTMPPCl-related catalysts. In the ESI, Fig. S3,† the physical characterizations of the H_2/Fe ± S catalysts are shown.

From XRD and Mößbauer measurements of the Fe/Fe − S and H_2/Fe − S catalysts, graphite, elemental iron and cohenite can be identified. Apparently, without sulfur-addition the formed iron by-products are hardly accessible during the acid leaching. As can be seen in Fig. S4† for the Fe/Fe − S catalysts these particles are covered by some graphene layers that protect them against the acid attack.

In accord with the XRD data the Raman measurements (Fig. 3b and S3b†) visualize a higher degree of graphitization of the sulfur-free catalysts (Fe/Fe − S and H_2/Fe − S) as indicated by the higher intensity and smaller full-width at half-maximum of the G-band (and D-band) in comparison to the sulfur-containing catalysts (Fe/Fe + S and H_2/Fe + S). The extensions of the graphene-layers, as calculated from the ratio of D-to-G-peak intensities, are higher for the sulfur-containing catalysts. The diffractograms of the sulfur-added catalysts exhibit predominantly X-ray amorphous behaviour indicating the good solubility of all crystalline iron phases (basically troilite) in acid that were formed until the end of the heat treatment step.

In Table 1 the results of the chemical composition from bulk-elemental analysis of the catalysts and their [N]/[Fe] ratios are summarized. In agreement with the XRD results the sulfur-free preparation results in a high amount of residual iron whereas the preparation approaches with sulfur lead to low iron concentrations. In contrast, the amount of nitrogen is drastically lower for the sulfur-free catalysts compared to the sulfur-added ones although it was the same in all precursor mixtures (only the porphyrin worked as the nitrogen source).

It is important to note that indicated by a ratio of [N]/[Fe] > 4 the overall iron could be present in FeN_4-centers for both sulfur-added catalysts. From Mößbauer spectroscopy it can be deduced that there is a small contribution of superparamagnetic iron (yellow singlet), which means that iron is not exclusively present in FeN_4-centers. In contrast, the number of FeN_4-centers in the sulfur-free catalysts is limited by their low nitrogen concentrations. In the best case, only one third of the number of active sites compared to the sulfur-containing catalysts have been formed.

III. Effect of sulfur on the electrochemical performance of the final catalysts

Fig. 4 gives the cyclic voltammograms (a) and kinetic current density calculated from Levich analysis (b) as a function of the

Table 1 Summary of the atomic concentrations calculated from NAA and combustion analysis. The mass-related concentration of oxygen was first calculated assuming it as the difference to 100 wt%. The error is <10% for all elements except hydrogen (error bar 10–20%)

at%	Fe	N	C	H	S	O	Ratio N/Fe
Fe/Fe + S	0.66	3.57	70.62	11.89	0.94	12.31	5.4
H_2/Fe + S	0.66	4.11	75.85	6.30	1.84	11.24	6.2
Fe/Fe − S	1.95	0.91	84.4	6.91	0.16	3.95	0.5
H_2/Fe − S	1.71	1.17	78.5	9.23	0.13	9.28	0.7
Fe/KB600	0.22	1.28	92.67	2.1	0.17	3.52	5.8

applied potential for both sample series (Fe/Fe ± S and H_2/Fe ± S). It can easily be recognized that the capacity is larger for both sulfur-added catalysts in comparison to the sulfur-free preparations. Furthermore, induced by sulfur-addition more than a 10 fold higher kinetic current density was reached and the onset potential (defined as U at −0.05 mA cm^{-2}, see Fig. S5† for RDE measurements) was shifted from 0.69 V to 0.79 V and from 0.71 V to 0.79 V, respectively, for the Fe/Fe and H_2/Fe catalysts.

As a reference, the electrochemical data of Fe/KB600 prepared at the same heat treatment temperature are additionally shown in Fig. 4 (see the Experimental part for details of its preparation). The kinetic current density of this catalyst (which is free of sulfur) is from the same order of magnitude as the sulfur-added catalysts. For that reason, the high activities of Fe/Fe + S and H_2/Fe + S catalysts are not due to the sulfur-addition but the addition of sulfur prevents a negative effect that appears without it. (Please note: the catalysts prepared by the oxalate-supported pyrolysis can easily be enhanced by subsequent heat-treatment steps to achieve current densities of 9 mA cm^{-2} (at 0.8 V).[18] However, second heat treatment of the reference catalyst in either an N_2 or NH_3 atmosphere led only to a factor of 1.5 higher current densities, compare with Fig. S6.†)

To further support this argument, the results of bulk-elemental analysis of this reference catalyst are added in Table 1. As iron and nitrogen (from the porphyrin) are only present on the surface of the carbon support the overall concentrations of both elements are smaller compared to the other catalysts. The ratio [N]/[Fe], however, is similar to both catalysts prepared by adding sulfur to the precursor mixture.

Discussion

I. Role of sulfur during the pyrolysis process

We have seen that on the one hand similar to the CoTMPP-based system also for the oxalate-supported pyrolysis in the presence of FeTMPPCl or H_2TMPP an improved performance can be recognized when the precursors are prepared with sulfur-addition. On the other hand, the comparison to the impregnation catalyst Fe/KB600 prepared by impregnation of a carbon black indicates that the higher catalytic activities of Fe/Fe + S and H_2/Fe + S are not related to an improving effect by the addition of sulfur.

It is well-known that iron catalyses the formation of graphite during high-temperature treatments.[23] In a first step, an amorphous carbon is dissolved in iron or iron-carbide particles. When the solvent gets supersaturated or is quenched, this carbon is precipitated as graphite.[24] The iron is understood as a transport medium whereas the change in free energy from disordered carbon to graphitic carbon is the driving force.[24] Hence, it can be concluded that the neighboured carbon planes (with the integrated catalytic FeN_4-centers) are somehow captured by the iron particles that are formed as the final product of the iron oxalate decomposition under a reducing atmosphere (because of the carbon from the porphyrins).

When sulfur is added to the precursor mixture sulfur adsorbs on the iron particles (and iron sulfide is formed during the heat-treatment). Consequently, the agent responsible for the graphitization cannot be formed so that the graphite forming process is inhibited, as described in the literature.[25] As a consequence a larger number of catalytic sites remain intact. As no continuous release of HCN-fragments appears (related to the decomposition of active sites) the main FeN_4-decomposition must be assigned to the formation process of iron carbide itself. Since troilite reveals good solubility in HCl this inactive by-product can easily be removed by the final acid leaching.[26]

II. Effect of sulfur on the ORR activity

Related to the results in Table 1 and the discussion of the pyrolysis process it can be concluded that without sulfur-addition a higher amount of active sites (FeN_4) are destroyed during the initial iron-carbide formation leading to a smaller ORR current density.

However, comparing the Mößbauer results and the results from bulk-elemental analysis in Table 1 of sulfur-free and sulfur-added catalysts, it becomes clear that the increase in kinetic current density is much higher than the increase in the number of active FeN_4-centers. A direct contribution of sulfur in gaining ORR activity can be excluded as the second heat treatment of the Fe/Fe + S catalysts in ammonia or forming gas leads to complete removal of sulfur without having a negative effect on the ORR activity. Three different effects might cause the disproportionate increase of kinetic current density:

(1) The formation of iron sulfide in the pyrolysis of the sulfur-added samples leads to an amorphous carbon (see XRD in Fig. 3 and S3†) that enables a higher electrochemical active surface area (Fig. 4a). Hence, a larger number of FeN_4-centers might be accessible during ORR.

(2) The higher doping of the carbon with nitrogen-heteroatoms (estimated from Table 1) could promote the oxygen reduction reaction and enable a higher turn-over frequency (TOF) of the sulfur-added catalysts, as suggested by theoretical calculations and heat-treated carbon-supported FeTMPPCl-based catalysts.[13,27]

(3) The larger graphene-layer extensions could enable an improved electronic environment that allows a faster ORR (higher TOF).[14]

III. Avoidance of carbide-formation by performing an intermediate acid leaching

From Fig. 2 and S1† it is clear that iron-carbide formation and the disintegration of active sites take place at temperatures >550 °C if an excess of iron is present in the precursor mixture. Therefore, an alternative preparation route to prevent the decomposition of FeN_4-centers induced by iron-carbide formation should be the interruption of the pyrolysis process after reaching the temperature of 500 °C (see the Experimental part for the details of this preparation).

The performance of an intermediate acid leaching after quenching of the sample from 500 °C to RT for the removal of excess iron should enable minimizing carbide formation in the further consecutive heat treatment process. We tried this variation of the standard oxalate-supported pyrolysis of FeTMPPCl (catalysts have the addition of IAL (intermediate acid leaching)

to their label). As can be seen from the electrochemical data in Fig. 5, these catalysts exhibit indeed a similar catalytic performance compared with the sulfur-containing standard catalyst. Therefore, the interruption of the pyrolysis process with an IAL also allows obtaining similar high current densities to catalysts prepared under sulfur-addition.

With a view to the literature and the structural characterization of Fe–N–C catalysts discussed in those studies, it becomes clear that most of the catalysts (especially when prepared at higher temperatures) are characterized by the presence of iron carbide.[3,28–33] Hence, we believe that (i) with the optimized addition of sulfur to the precursor mixture in the preparation processes or (ii) by performing an intermediate acid leaching several catalysts can be enhanced in terms of concentration of active sites and ORR activity.

As sulfur residuals could work as poison during the FC run, especially this second approach might be of interest for the preparation of well-performing catalysts.

Conclusions

The oxalate-supported pyrolysis of FeTMPPCl or H_2TMPP enables the preparation of highly active ORR catalysts. On the basis of *in situ* high-temperature X-ray diffraction (HT-XRD) and thermogravimetry coupled with mass-spectroscopy (TG-MS) the reasons for the better performance of sulfur-added catalysts were elucidated. The sulfur has no beneficial effect by itself, but it prevents iron-carbide formation during the heating process. As shown by the combination of HT-XRD and TG-MS, the formation of iron carbide causes disintegration of FeN_4-centers that are known to be responsible for the ORR activity of these Fe–N–C catalysts. Structural characterization of the final catalysts confirms the much lower concentration of FeN_4-centers in the catalysts prepared without sulfur-addition.

On the basis of the performed characterization two options for the enhancement of active site densities of Fe–N–C catalysts can be derived:

(1) Addition of sulfur to the precursor mixture.

(2) Performance of an intermediate acid leaching to remove excess iron.

As iron carbide is often found as a by-product in the preparation of Fe–N–C-catalysts *via* different approaches we believe that our results have a large impact on the optimization of active site densities (and thus performance) of these catalysts.

Acknowledgements

TG-MS measurements were performed at the Institut für Kristallzüchtung IKZ with the help of Dr Klimm. Sven Kubala (now FHI) was of great support for his substantial contribution in adapting the HT-XRD measuring cell to the harsh *in situ* reaction environment. Bulk-elemental analysis and NAA were performed by Prof. Linker and Dr Alber, respectively. Mößbauer spectroscopy was performed with the help of Prof. em. Abs-Wurmbach at the Institute of Technology Berlin. Their help for the fruitful development of these data is greatfully acknowledged. Furthermore, we would like to thank the BESSY team for the comprehensive technical support during beam time.

Notes and references

1 A. de Frank Bruijn and G. J. M. Janssen in *Encyclopedia of Sustainable Science and Technology*, ed. R. A. Meyers, Springer, NY, 2013, p. 7694.
2 M. Lefèvre, E. Proietti, F. Jaouen and J.-P. Dodelet, *Science*, 2009, **324**, 71.
3 E. Proietti, F. Jaouen, M. Lefévre, N. Larouche, J. Tian, J. Herranz and J.-P. Dodelet, *Nat. Commun.*, 2011, **2**, 416.
4 G. Wu, K. L. More, C. M. Johnston and P. Zelenay, *Science*, 2011, **332**, 443.
5 P. Bogdanoff, I. Herrmann, M. Hilgendorff, I. Dorbandt, S. Fiechter and H. Tributsch, *J. New Mater. Electrochem. Syst.*, 2004, **7**, 85.
6 I. Herrmann, U. I. Kramm, S. Fiechter and P. Bogdanoff, *Electrochim. Acta*, 2009, **54**, 4275.
7 I. Herrmann, U. I. Kramm, J. Radnik, P. Bogdanoff and S. Fiechter, *J. Electrochem. Soc.*, 2009, **156**, B1283.
8 U. I. Koslowski, I. Abs-Wurmbach, S. Fiechter and P. Bogdanoff, *J. Phys. Chem. C*, 2008, **112**, 15356.
9 U. I. Kramm, I. Herrmann-Geppert, P. Bogdanoff and S. Fiechter, *J. Phys. Chem. C*, 2011, **115**, 23417.
10 H. Tributsch, U. I. Koslowski and I. Dorbandt, *Electrochim. Acta*, 2008, **53**, 2198.
11 U. I. Koslowski, I. Herrmann, P. Bogdanoff, C. Barkschat, S. Fiechter, N. Iwata, H. Takahashi and H. Nishikoro, *ECS Trans.*, 2008, **13**, 125.
12 U. I. Kramm, I. Herrmann, S. Fiechter, G. Zehl, I. Zizak, I. Abs-Wurmbach, J. Radnik, I. Dorbandt and P. Bogdanoff, *ECS Trans.*, 2009, **25**, 659.
13 U. I. Kramm, I. Abs-Wurmbach, I. Herrmann-Geppert, J. Radnik, S. Fiechter and P. Bogdanoff, *J. Electrochem. Soc.*, 2011, **158**, B69.
14 I. Herrmann, PhD thesis, Freie Universität, Berlin, 2006.
15 M. Ferrandon, A. J. Kropf, D. J. Myers, K. Artyushkova, U. I. Kramm, P. Bogdanoff, G. Wu, C. M. Johnston and P. Zelenay, *J. Phys. Chem. C*, 2012, **116**, 16001.
16 O. Contamin, C. Debiemme-Chouvy, M. Savy and G. Scarbeck, *Electrochim. Acta*, 1999, **45**, 721.
17 T. D. Hatchard, J. E. Harlow, K. M. Cullen, R. A. Dunlap and J. R. Dahn, *J. Electrochem. Soc.*, 2010, **159**, B121.
18 F. Jaouen, J. Herranz, M. Lefèvre, J.-P. Dodelet, U. I. Kramm, I. Herrmann, P. Bogdanoff, J. Maruyama, T. Nagaoka, A. Garsuch, J. R. Dahn, T. S. Olson, S. Pylypenko, P. Atanassov and E. A. Ustinov, *ACS Appl. Mater. Interfaces*, 2009, **1**, 1623.
19 U. I. Kramm, G. Zehl, I. Zizak, I. Herrmann, I. Dorbandt, P. Bogdanoff and S. Fiechter, *Bessy Annual Report* 2008, pp. 39–41.
20 F. Tuinstra and J. L. K. önig, *J. Chem. Phys.*, 1970, **53**, 1126.
21 I. Herrmann, U. I. Kramm, S. Fiechter, V. Brüser, H. Kersten and P. Bogdanoff, *Plasma Processes Polym.*, 2010, **7**, 515.

22 A. F. Holleman and E. Wiberg, *Lehrbuch anorg. Chem.*, Walter de Gruyter & Co, Berlin, 1960, vol. 47–56.
23 K. Kinoshita, *Carbon – Electrochem. Physicochem. Properties*, Wiley-Interscience, 1st edn, 1987.
24 H. Marsh and A. P. Warburton, *J. Appl. Chem.*, 1970, **20**, 133.
25 H. J. Grabke, D. Moszynski, E. M. Müller-Lorenz and A. Schneider, *Surf. Interface Anal.*, 2002, **34**, 369.
26 P. Ramdohr and H. Strunz, *Klockmanns Lehrbuch der Mineralogie*, Ernst Klett Verlag, Stuttgart, 1978/1980, vol. 16.
27 V. V. Strelko, V. S. Kuts and P. A. Thrower, *Carbon*, 2000, **38**, 1499.
28 A. Garsuch, R. d'Eon, T. Dahn, O. Klepel, R. R. Garsuch and J. R. Dahn, *J. Electrochem. Soc.*, 2008, **155**, B236.
29 G. Liu, X. Li, P. Ganesan and B. N. Popov, *Appl. Catal., B*, 2009, **93**, 156.
30 S.-H. Liu and J.-R. Wu, *Microporous Mesoporous Mater.*, 2013, **170**, 150.
31 H. Meng, N. Larouche, M. Lefèvre, F. Jaouen, B. Stansfield and J.-P. Dodelet, *Electrochim. Acta*, 2010, **55**, 6450.
32 J. Wu, W. Li, D. Higgins and Z. Chen, *J. Phys. Chem. C*, 2011, **115**, 18856.
33 U. I. Kramm, M. Lefèvre, N. Larouche, D. Schmeisser, J.-P. Dodelet, *J. Am. Chem. Soc.*, 2014DOI: 10.1021/ja410076f.